Statistical diagnosis of a gas-solid fluidized bed using Electrical Capacitance Tomography.

Christo Rautenbach, Morten C. Melaaen and Britt M. Halvorsen

Institute for Process, Energy and Environmental Technology
Telemark University College
Norway
T: +47 3557 5222; E: christo.rautenbach@hit.no

Abstract

Fluidization experiments were performed using several particle size distributions of spherical glass particles, ranging from Geldart B to D. An Electrical Capacitance Tomography (ECT) tomograph was utilised in the present study and its usefulness as a diagnostic tool is illustrated. During the experiments a 10.4*cm* diameter tower was utilised and the tower was operated at atmospheric pressure and room temperature (cold fluidized bed). Statistical analysis were performed on the average solid fraction data obtained using the ECT tomograph. Using the time domain skewness and kurtosis the time series could be characterised and the quality of fluidization is determined at different superficial gas velocities (Azizpour, H., Sotudeh-Gharebagh, R., Zarghami, R., Abbasi, M., Mostoufi, N., and Mahjoob, M. (2011). Characterization of gas-solid fluidized bed hydrodynamics by vibration signal analysis. *International Journal of Multiphase Flow*, 37:788-793). Statistical analysis is also used to characterise the influence of small particles on the bed hydrodynamics.

Keywords: ECT, Gas-solid fluidization, particle size distribution, fluidization quality, skewness, excess kurtosis

1. Introduction

Fluidized bed reactors are used in a variety of industrial applications including Chemical Looping Combustion (CLC) and Biomass gasification. The efficiency of gas-solid fluidized bed reactors depends on the mixing of the gas and solids and even though these reactors are very successful they do present some limitations (Azizpour et al. 2011, Saxena et al. 1993). De-fluidization is one of the problems that may occur in fluidized beds due to changes in the hydrodynamics of the bed during operation (Azizpour et al. 2011). Therefore it is important to understand the complex hydrodynamics of fluidized beds and to be able to monitor the quality of fluidization under various operating conditions.

The quality of fluidization can be described in terms of the uniformity of distribution of the fluidizing gas (Patel et al. 2008). Several measurement techniques have been utilised in the past to investigate the quality of fluidization or the gas maldistribution in a fluidized bed. These techniques include pressure probe measurements (Saxena et al. 1993, Lin and Wey 2004), temperature probe measurements (Saxena et al. 1993), γ-ray tomography and acoustic measurements (Azizpour et al. 2011, Salehi-Nik et al. 2009). The different measurements techniques have different advantages and disadvantages and can be used to diagnose the quality of fluidization. In the work done by Lin et al. (2004) the quality of fluidization was described using the fluidization index. The fluidization index used by Lin et al. (2004) is modified from its original form and was used to describe good or bad bed behaviour in terms of the pressure fluctuations in the bed. The fluidization index can also be related to the maldistribution factor, χ, used in the work done by Patel et al. (2008) and Loser (1999). The maldistribution factor can be defined for pixilated solid fraction images and is defined as

$$\chi = \frac{1}{n}\sum_{i=1}^{n}\left(\frac{\alpha_i - \overline{\alpha}}{\overline{\alpha}}\right), \tag{1}$$

where n denotes the number of pixels in the particular image (tomogram), α_i is the solid fraction of a particular pixel and $\overline{\alpha}$ is the solid fraction of the entire image or reactor cross-section (Patel et al. 2008). Alternatively pressure frequency and magnitude have been used to

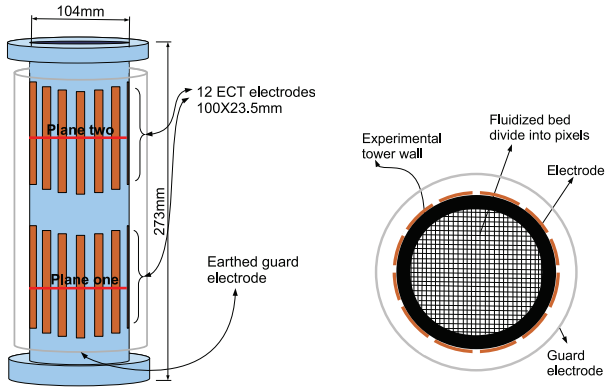

(a) (b)

Figure 1: A schematic drawing of the two plane ECT tomograph utilised in the present study. (a) The two measuring planes of the system are indicated together with the electrodes and earthed guard screen. (b) A cross-sectional view of the ECT sensor together with the 1024 pixels created by the reconstruction program.

access the quality of fluidization (Lin and Wey 2004). Good quality fluidization can be obtained by keeping pressure fluctuation as small and frequent as possible as this will indicate numerous small bubbles (Lin and Wey 2004). Statistical methods in combination with the fluidization index and the maldistribution factor, χ, have been successfully used to diagnose the fluidization quality in fluidized beds (Saxena et al. 1993, Lin and Wey 2004, Salehi-Nik et al. 2009). Since these methods have successfully been used with pressure fluctuation measurements it appears feasible to do the same analysis with solid fraction fluctuation measurements obtained with the ECT tomograph. Pressure fluctuations are an indirect indication of the solid fraction fluctuation in the bed and by using the ECT tomograph the entire cross-section of the bed is taken into account as oppose to only a probe volume (Makkawi and Wright 2002). A pressure probe is usually located at the bed wall and according to Saxena et al. (1993) the probe will only register damped pressure fluctuations that reaches the bed wall. By using the ECT tomograph the entire cross-section of the bed is taken into account. Viewing the entire cross-section of the experimental reactor will give a better representation of the dynamic behaviour of the bed. The data obtained with the ECT tomograph can also be viewed as images which can be used to confirm the behaviour deduced from the statistical analysis.

The importance of particle size distributions is well described in literature (Lin and Wey 2004, Jayarathna and Halvorsen 2009) and more recent studies investigated the influence of small particles on the overall bed behaviour in a 2D bed using photographic methods (van Biljon et al. 2011). To examine the effect of small particles on the overall bed behaviour in a 3D bed, various amounts of small particles were mixed into the powder of larger particles used in the experiments.

The aim of the present study was to use statistical methods to diagnose the quality of fluidization for four different mixtures of spherical glass particles and to illustrate the usefulness of the ECT tomograph for this purpose. The influence of small particles on the overall bed hydrodynamics, were also investigated. The analysis was performed on cross-sectional solid fraction data obtained with a ECT tomograph at two bed heights.

2. Experimental

2.1. Measurement apparatus, ECT tomograph

A two plane ECT tomograph was utilised in the present study. It consists of two arrays of electrodes each array containing twelve electrodes. In Figure 1 a schematic drawing of the ECT sensor is given. The location and size of the electrodes were designed by Process Tomography Ltd. (2003). As the sensor works with a soft field, it is very susceptible to external interference and thus the sensor is covered by a grounded screen to

protect the electrodes from external noise. The non intrusive design of the sensor can be observed in Figure 1. The electrodes are placed on the circumference of the experimental tower and does not influence the flow behaviour.

The ECT tomograph produces a cross-sectional image showing the distribution of electrical permittivities of the content of the experimental tower (Makkawi and Wright 2004). The capacitance reading is taken between each set of electrodes and produces $E\,(E-1)\,/2$ different measurements for one image that is reconstructed. E represents the number of electrodes used in the ECT sensor. These measurements are interpreted and illustrated as a colourful image using the Linear Back Projection (LBP) reconstruction algorithm. An example of such an image is provided in Figure 2. The resolution of the image is usually relatively low but can be sampled at high sample rates (low spatial resolution but high temporal resolution). Off-line image processing can also improve the quality of the image (Makkawi and Wright 2002) but the present study investigated the use of only on-line measurements. The measuring

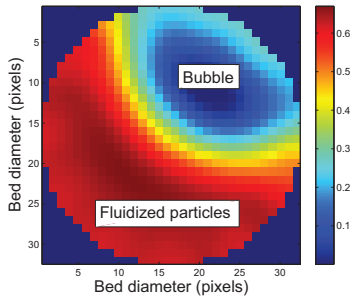

Figure 2: A cross-sectional image of the experimental tower indicating the solid fraction values inside the tower at a particular plane. Red indicates particles at minimum fluidization conditions and blue indicates air.

planes are located at two different locations. The heights in the fluidized bed will be denoted by H_m, the tower diameter by D and the static bed height by H. The first plane is located at a height of $15.65cm$ ($H_m/D = 1.5$) and the other at a height of $28.65cm$ ($H_m/D = 2.8$) above the porous plate distributor. The lower plane will be called *plane one* and the upper plane, *plane two* (refer to Figure 1 (a)). Even though the ECT tomograph calculates average solid fraction values the data that are obtained are viewed as a slice through the bed at the center of each electrode. Due to the reconstruction program the measurements are most accurate close to the center plane of the electrodes. Plane one and plane two are thus located at the center position of the electrodes (refer to Figure 1 (a)). Some validation of the ECT tomograph has been done and it was shown that the ECT tomograph gives relatively accurate results when a known volume of a dielectric object could be measured with the ECT tomograph (Warsito and Fan 2005, Sharma et al. 2010, McKeen and Pugsley 2002, Pugsley et al. 2003).

Research done by Makkawi et al. (2004) revealed that using ECT to measure dynamic parameters such as the standard deviation of the average solid fraction fluctuation and the bubble velocity or frequency, a minimum measuring span of $60s$ must be implemented. Thus using a sampling rate of $100Hz$ and an experimental span of $60s$, 6000 images can be produced. Up to 8000 images can be produced in one experimental span (depending on the number of electrodes, computing power and speed of the reconstruction algorithm) (Makkawi and Wright 2004). For the remainder of this study a measuring span of $60s$ were implemented.

2.2. *Experimental configuration and parameters*

To investigate the influence of small particles on the hydrodynamics of a fluidized bed a range of different particle sizes were mixed. During the course of the present study the $100-200\mu m$ particles will be the smallest particle size distribution used and was mixed with powders of larger size distributions. The mixtures that were investigated are presented in Table 1. Each of the mixtures had different percentages of small particles. Investigating these mixtures provided valuable results related to the influence of small particles on fluidized bed hydrodynamics. The mean particle diameter was calculated using the *surface-volume mean* diameter and is defined as

$$\overline{d}_{sv} = \frac{1}{\sum_i x_i/d_i}, \tag{2}$$

with x_i the mass fraction of the particular particle size, d_i. The particles were spherical glass particles with an approximate density of $2485kg/m^3$. Compressed air was used as fluidizing fluid. The experimental tower had a diameter of $D = 10.4cm$ and a height of $1.5m$. The $100-200\mu m$ particles and *mix 1* (refer to Table 1) was classified as Geldart B particles while the $750-1000\mu m$ particles and *mix 2* were classified as Geldart D particles. The difference in behaviour of these particles will be made clear in the statistical diagnosis of the different particle size distributions.

Table 1: Relevant parameters of the powders and experimental tower used in the present study.

Particle size distribution	Mean particle size ($\overline{d}_{sv}$) [μm]	Solid fraction (ϵ_s) [-]	H/D [-]	u_{mf} [m/s]	Distributor
100 – 200μm	153	0.68	4.6	0.02	porous plate
400 – 600μm	482.9	0.68	—	0.21	porous plate
750 – 1000μm	899.15	0.67	4.4	0.45	porous plate
mix 1: 50% 100 – 200μm, 50% 400 – 600μm	265.58	0.66	4.6	0.04	porous plate
mix 2: 8.5% 100 – 200μm, 8.5% 400 – 600μm, 83% 750 – 1000μm	800.35	0.7	4.7	0.27	porous plate

3. Theory; Sample skewness and sample excess kurtosis

For a sample of N measurements the **sample skewness** (SS) can generally be defined as

$$SS = \frac{\frac{1}{N}\sum_{i=1}^{N}\left(\phi_{si} - \overline{\phi}_s\right)^3}{\left(\frac{1}{N}\sum_{i=1}^{N}\left(\phi_{si} - \overline{\phi}_s\right)^2\right)^{3/2}}, \tag{3}$$

where ϕ_{si} represents the average solid fraction across the bed at a certain height and at a given time interval (i), $\overline{\phi}_s$ represents the average of all the cross-sectional average solid fraction values and N is the total number of measurements taken. Thus $\overline{\phi}_s$ can be expressed as

$$\overline{\phi}_s = \left(\sum_{i=1}^{N}\phi_{si}\right)/N. \tag{4}$$

The skewness of a sample is a measure of the asymmetry of the sample. The skewness of a sample can be positive, negative or undefined. If the skewness of a sample is negative it indicates that the sample distribution had a longer 'tail' on the left side of the distribution. This kind of distribution is also called *left*-skewed (Scheffé 1959). This implies that the bulk of the values in the probability density function lies to the right of the distribution, including the median. The concept of skewness is illustrated in Figure 3 with two schematic probability density functions. The median is the midpoint of a distribution separating the low and high values of the distribution and will be indicated by $\widetilde{\phi}_s$. For a positive skewness value the opposite is true and the sample distribution will have a longer 'tail' on the right side of the median and thus the bulk of the values in the distribution will be on the left side of the distribution. This distribution is called *right*-skewed and the mean will be on the right side of the median.

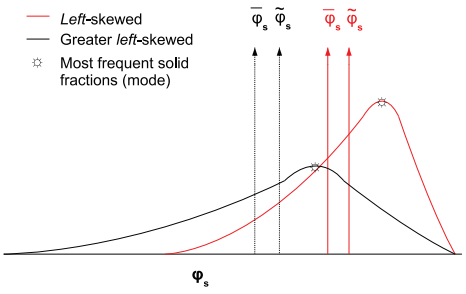

Figure 3: Schematic figure depicting two left-skewed distributions with different degrees of skewness. The mean of the distribution is represented by $\overline{\phi}_s$ and the median is indicated by $\widetilde{\phi}_s$.

Another useful tool in data analysis is the kurtosis of a sample. For a sample of N values the **sample excess kurtosis** (SEK) can be defined as

$$SEK = \frac{\frac{1}{N}\sum_{i=1}^{N}\left(\phi_{si} - \overline{\phi}_s\right)^4}{\left(\frac{1}{N}\sum_{i=1}^{N}\left(\phi_{si} - \overline{\phi}_s\right)^2\right)^2} - 3, \tag{5}$$

with the same variable definitions described in equation (3). This definition of the kurtosis is known as the *excess kurtosis* where the '*minus 3*' is added to make the kurtosis of a normal distribution equal to zero. One of the best ways to describe the kurtosis of a distribution is probably to refer to it as the '*peakedness*' or inversely

the '*flatness*' about the mean of a distribution (Lin and Wey 2004).

Distributions that has a excess kurtosis value of zero is called **mesokurtic**. A trivial example of such a distribution is the normal distribution. Next a distribution with a positive excess kurtosis value is called **leptokurtic**. This would typically be a distribution with more extreme peaks and thus not a generally 'flat' distribution. A distribution with a negative excess kurtosis is called **platykurtic** and is typical of a visually 'flat' distribution with almost no extreme deviations in the distribution (Scheffé 1959). In Figure 4 a schematic illustration is given to explain the concept of kurtosis.

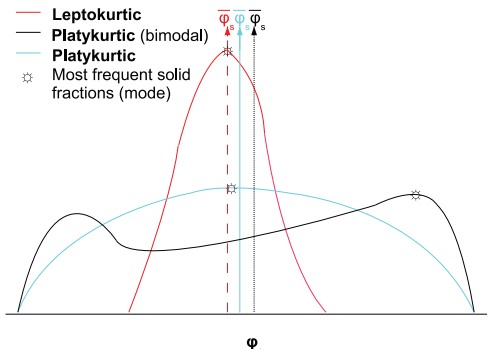

Figure 4: Schematic figure depicting the concept of kurtosis via three different probability density functions. The average of the distribution is represented by $\bar{\phi}_s$.

4. Results and discussion

To investigate the fluidization quality, the skewness and excess kurtosis of the four particle mixtures were investigated. The measurements were taken at two different bed heights, the one measuring plan was at a height of $H_m/D = 1.5$ and the other at $H_m/D = 2.8$, as mentioned in Section 2.1. In Figure 5 the skewness values are given for each of the four particle size distributions at $H_m/D = 1.5$. All of the powders had decreasing skewness values as the superficial velocity increased. The different particle groups are also easy to distinguish (as illustrated in Figure 5). The Geldart B particles had approximately linear decreasing skewness values while the Geldart D particles had more of a quadratic behaviour. Lin and Wey (2004) also used statistical methods to analyse pressure measurements in a

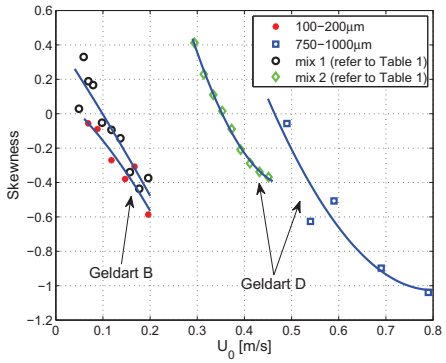

Figure 5: Skewness values as a function of the superficial velocity, U_0, at $H_m/D = 1.5$. Based on the probability density function of average solid fraction values recorded with a ECT tomograph.

fluidized bed. According to Lin and Wey (2004) an increasing skewness indicates that multiple small bubbles are present at the particular measuring height. Numerous small bubbles are desirable in a bubbling fluidized bed as it cause more efficient mixing of solids and better mass transfer properties than too larger bubbles (Saxena et al. 1993). The decreasing skewness with increasing superficial velocity (given in Figure 5) thus indicates that the bubbles has a long enough residence time in the bed to coalesce into larger bubbles at $H_m/D = 1.5$ (Lin and Wey 2004). In both particle groups the powders with the widest particle size distributions produced generally higher skewness values (*mix 1* and *mix 2* produced the widest particle size distributions). At a height of $H_m/D = 1.5$ the wide particle size distribution thus creates a bed that can be characterised by smaller bubbles compared to that of the narrower particle size distributions. When the skewness values go from positive to negative it indicates that the bubbling bed has transferred from micro- to macro-structures (Azizpour et al. 2011). This also explains why the powders containing the smaller particles have higher skewness values. The finer structures are more important in the finer powders leading to higher skewness values (Azizpour et al. 2011).

Generally Lin and Wey (2004) stated that the fluidization index increases with an increase in superficial velocity and therefore the quality of fluidization decreases with an increase of the superficial velocity. When the fluidization index becomes too large it is an indication of the onset of the slugging regime (Lin and Wey

2004). Hence a decreasing skewness is an indication of a progressively decreasing fluidization quality and the introduction of small particles (and thus wide particle size distribution) increases the fluidization quality. The positive attributes of small particles in a particle size distribution was also noted by Kunii and Levenspiel (1991). They stated that the quality of fluidization can be spectacularly improved by adding a small amount of small particles to act as lubricant (Kunii and Levenspiel 1991).

In Figure 6 the same data is presented as in Figure 5 but as a function of a dimensionless coefficient. The di-

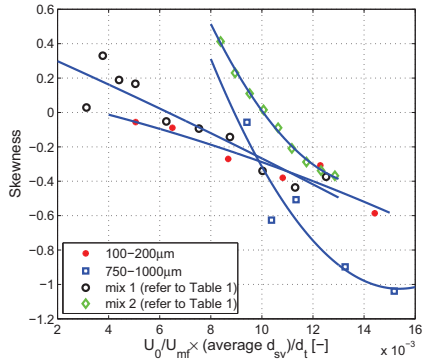

Figure 6: Skewness values as a function of the dimensionless coefficient, $U_0/U_{mf} \times \overline{d}_{sv}/d_t$, at $H_m/D = 1.5$. Based on the probability density function of average solid fraction values recorded with a ECT tomograph.

mensionless coefficient used in the present study is the product of the fluidization number, U_0/U_{mf}, and the ratio of the surface-volume mean diameter and the tower diameter, $\overline{d}_{sv}/d_t$. The dimensionless coefficient takes into account the mean particle size as small particles with a wide size distribution can be fluidized in a wider range of gas flow rates (Kunii and Levenspiel 1991). Thus to account for this phenomena and to view the statistical values on a more convenient way, this coefficient will be used in the remainder of the study. From Figure 6 it can also be observed that the $750-1000\mu m$ powder produced the lowest skewness values as the superficial velocity was increased. This powder was therefore clearly prone to slugging and spouting and thus bad fluidization quality. This could be expected for large particles of a narrow size distribution (Kunii and Levenspiel 1991). The influence of the small particles in the *mix 2* powder can also be observe in Figure 6 as it produced larger skewness values than when just the $750-1000\mu m$ powder was used. Azizpour et al. (2011) did experiments with acoustic signals and pressure measurements in fluidized beds filled with sand. They stated that the skewness will decrease as the average particle size is increased (Azizpour et al. 2011). This is also confirmed for the Geldart D particles size distributions in Figure 6. Generally, adding small particles seems to increase the skewness values.

In Figure 7 the excess kurtosis values are given at $H_m/D = 1.5$. Azizpour et al. (2011) stated that the

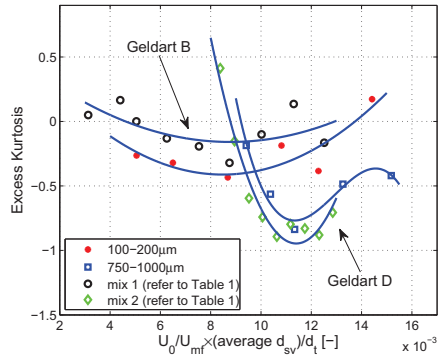

Figure 7: Excess kurtosis values as a function of the dimensionless coefficient, $U_0/U_{mf} \times \overline{d}_{sv}/d_t$, at $H_m/D = 1.5$. Based on the probability density function of average solid fraction values recorded with a ECT tomograph.

kurtosis of pressure fluctuation measurements reached a minimum against the superficial gas velocity and that this minimum occurs at higher superficial velocities for larger particles. Generally this behaviour is also observed in Figure 7 as the difference between Geldart B and D particles can clearly be noticed. The different Geldart groups behave differently. The Geldart B powders had a flat curve while the Geldart D particles had a clear minimum point. According to Azizpour et al. (2011) this minimum point in the kurtosis values is an indication of the change of the meso-structure of the bed and is not necessarily an indication of regime transition.

As mentioned before, Lin and Wey (2004) stated that decreasing skewness values mainly occurs higher up in a fluidized bed when the bubbles have a long enough residence time in the bed to coalesce and form larger bubbles and thus large pressure fluctuations. With the ECT average solid fraction measurements, large average solid fraction fluctuations are also an indication of large bubbles. Because of the decreasing skewness behaviour (shown in Figure 5 and 6) the minimum kurtosis

values observed in Figure 7 might indicate the onset of the slugging regime.

In Figure 8 the skewness values of the probability density function at $H_m/D = 2.8$ is provided. At

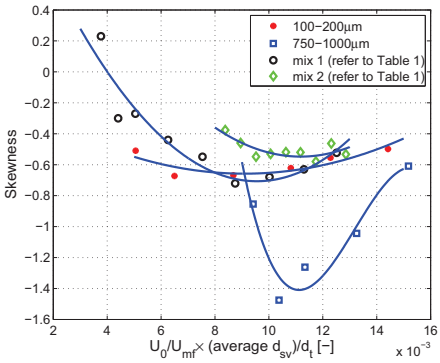

Figure 8: Skewness values as a function of the dimensionless coefficient, $U_0/U_{mf} \times \overline{d}_{sv}/d_t$, at $H_m/D = 2.8$. Based on the probability density function of average solid fraction values recorded with a ECT tomograph.

$H_m/D = 2.8$ the bubbles have had sufficient residence time in the bed to coalesce and form large bubbles. All of the investigated particle size distributions indicated a minimum skewness value at different superficial velocities. When the skewness values go from decreasing to increasing the bed must have reached the maximum bubble size as the variety of bubbles are increasing (Lin and Wey 2004). The coalescence and break down of bubbles are occurring simultaneously according Lin and Wey (2004), causing the skewness to increase again.

The influence of small particles are once again illustrated by the Geldart D particles in Figure 8. The skewness values of *mix 2* is much larger than just the $750 - 1000\mu m$ size distribution indicating better quality fluidization in the powder mixed with small particles.

In Figure 9 the excess kurtosis values at $H_m/D = 2.8$ is given. Figure 8 and 9 show that the values of skewness and kurtosis change inversely for three of the powders. The results given by Lin and Wey (2004), obtained with a Gaussian distribution with $\overline{d}_{sv} = 719\mu m$, also indicated that the kurtosis and skewness values (of pressure measurements) changed inversely. The excess kurtosis values of the *mix 2* powder was the only powder that had nearly the same trend as its skewness values. The gradient at which the $750 - 1000\mu m$ powder decreases in kurtosis values with increasing superficial velocity values is the greatest of all the powders and might

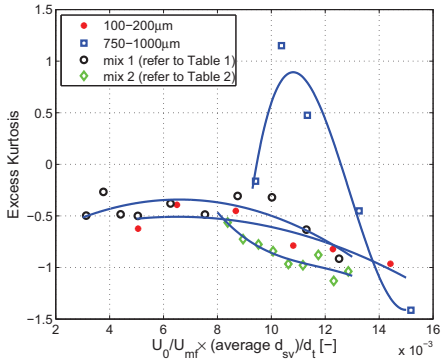

Figure 9: Excess kurtosis as a function of the dimensionless coefficient, $U_0/U_{mf} \times \overline{d}_{sv}/d_t$, at $H_m/D = 2.8$. Based on the probability density function of average solid fraction values recorded with a ECT tomograph.

indicate this Geldart D powder tends to slugging conditions. Again the *mix 2* and other finer powders indicate a less drastic variation in kurtosis values. These smooth changing kurtosis values might be an indication that the bed is still in the same regime. Saxena et al. (1993) stated that abrupt changes in skewness or kurtosis values indicate a regime change in the fluidized bed. Thus the small particles and the powders containing small particles perform better and are prone to better quality fluidization. This effect of small particles have been noted in literature before, where the introduction of small particles had the general effect of smaller bubbles in a bubbling fluidized bed (Rautenbach et al. 2011, van Biljon et al. 2011).

4.1. Visual diagnosis and confirmation of fluidized bed hydrodynamics

In the present study the usefulness of the ECT tomograph as a diagnostic tool in fluidized bed has been illustrated. It was show that the ECT tomograph could produce the same statistical diagnosis other popular measuring techniques can deliver. One of the advantages of the ECT tomograph is the possibility to produce solid fraction maps of the content of the reactor in a non intrusive manner. These images aids in diagnosing a fluidized bed alongside other diagnostic techniques.

In Figure 10 and 12 an example is presented of possible ECT tomograms. These images are time stacked tomograms indicating the solid fraction variation through the center of the bed for the firsts 5 seconds of the particular experiments. In these tomograms the difference

in bubble activity of plane one and two is also illustrated for three superficial velocities.

In Figure 10 the tomograms of the $750 - 1000\mu m$ powder is provided. As the superficial velocity is increased the clear slugging behaviour can be noticed in both plans. These slugs had a tendency to collapse and in Figure 11 this is illustrated by viewing the cross-section of the tower through a collapsing slug. In Figure 11 the solid particles in the center of the slug indicate the roof of the slug collapsing through the gas slug. These collapsing slugs also provide a possible explanation for the increase of bubble variety noted in Figure 6.

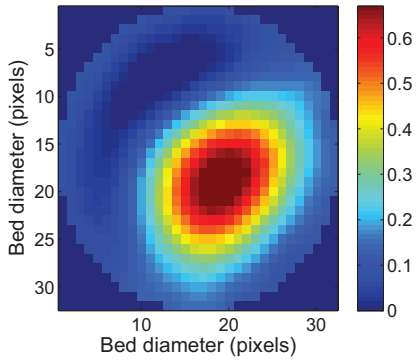

Figure 11: This is a cross-sectional image of the experimental tower at a superficial velocity of $0.79m/s$ at time $150cs$ of the 750-$1000\mu m$ powder at plane one. Refer to Figure 10.

In Figure 12 the tomograms of the *mix 2* powder is presented. The *mix 2* powder was selected as it clearly illustrated the influence of small particles when compared with the bubble behaviour in Figure 10. The small particles cause the bed to be characterise by smaller bubbles as the superficial velocity is increased together with a lowering of the minimum fluidization velocity. Previous studies also indicated that the small particles, in a particle size distribution, have the dominant effect on the minimum fluidization velocity (Jayarathna and Halvorsen 2009). From these results it is clear that small particles has a important influence on the overall bed hydrodynamics.

5. Conclusion

In the present study the usefulness of an ECT tomograph as a diagnostic tool in a fluidized bed was illustrated. Using statistical methods the quality of fluidization of a fluidized bed was assessed. Using these statistical methods the ECT tomograph proved to be equally effective at diagnosing the quality of fluidization compared to other popular measurement techniques used in industry. These methods include temperature probes, pressure probes and acoustic or vibration measurements.

The ECT tomograph together with the statistical analysis was employed to investigate the influence of small particles on the hydrodynamics of a fluidized bed. It was found that small particles had the general effect of smaller bubbles and better quality fluidization. These observations were also confirmed when compare with tomograms created from the ECT data. ECT thus provides an added advantage, above some other measurement techniques, by providing a non intrusive view of the flow behaviour alongside the other diagnostic techniques.

References

(2003). *PTL300-TP-G ECT system, Operation manual*. Process tomography Ltd., 86 Water Lane, Wilmslow, Cheshire. SK9 5BB, UK.

Azizpour, H., Sotudeh-Gharebagh, R., Zarghami, R., Abbasi, M., Mostoufi, N., and Mahjoob, M. (2011). Characterization of gas-solid fluidized bed hydrodynamics by vibration signal analysis. *International Journal of Multiphase Flow*, 37:788–793.

Jayarathna, C. and Halvorsen, B. M. (2009). Experimental and computational study of particle minimum fluidization velocity and bed expansion in a bubbling fluidized bed. Copenhagen, Denmark. International Conference of Scandinavian Simulation Society.

Kunii, D. and Levenspiel, O. (1991). *Fluidization Engineering*. Butterworth-Heinemann.

Lin, C. and Wey, M. Y. (2004). Statistical and power spectral analysis of quality of fluidization for different particle size distributions at high temperature. *Advanced Powder Technology*, 15(1):79–96.

Loser, T., Petritsch, G., and Mewes, D. (1999). Investigation of the two-phase countercurrent flow in structured packings using capacitance tomography. In *1st World Congress on Industrial Process Tomography*, pages 354–361, Greater Manchester.

Makkawi, Y. T. and Wright, P. C. (2002). Fluidization regimes in a conventional fluidized bed characterized by means of electrical capacitance tomography. *Chemical Engineering Science*, 57:2411–2437.

Makkawi, Y. T. and Wright, P. C. (2004). Electrical capacitance tomography for conventional fluidized bed measurements-remarks on the measuring technique. *Powder Technology*, 148:142–157.

McKeen, T. R. and Pugsley, T. S. (2002). The influence of permittivity models on the phantom images obtained from electrical capacitance tomography. *Measurement Science and technology*, 13:1822–1830.

Patel, A., Waje, S., Thorat, B., and Mujumdar, A. (2008). Tomographic diagnosis of gas maldistribution in gas-solid fluidized beds. *Powder Technology*, 185:239–250.

Pugsley, T., Tanfara, H., Malcus, S., Cui, H., Chaouki, J., and Winters, C. (2003). Verification of fluidized bed electrical capacitance tomography measurements with a fibre probe. *Chemical Engineering Science*, 58:3923–3934.

Rautenbach, C., Melaaen, M. C., and Halvorsen, B. M. (2011). Investigating the influence of fines in fluidized bed reactors using 3d ect

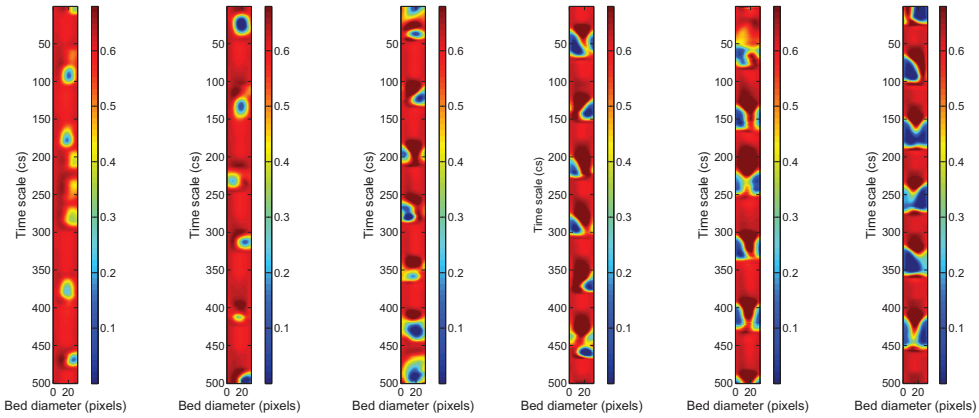

(a) Plane one (b) Plane two (c) Plane one (d) Plane two (e) Plane one (f) Plane two

Figure 10: The time staked images are given for the first 5s of each velocity using the 750-1000μm powder. The samples were at (a),(b) 0.5m/s, (c),(d) 0.64m/s and (e),(f) 0.79m/s respectively.

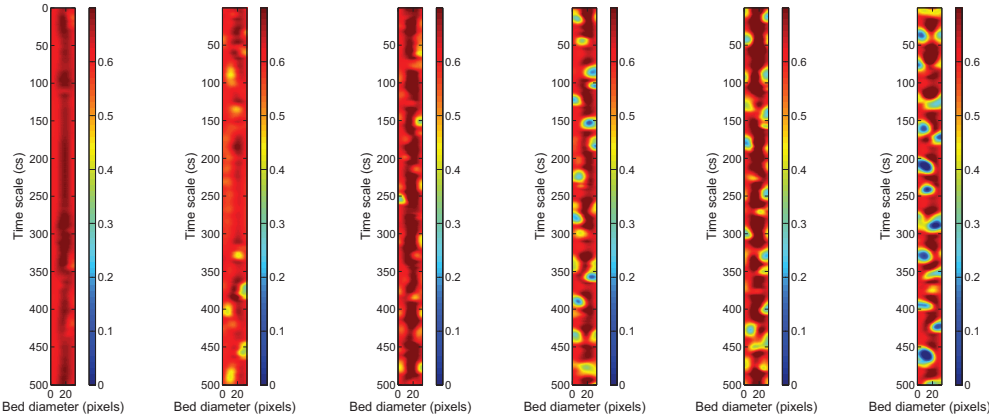

(a) Plane one (b) Plane two (c) Plane one (d) Plane two (e) Plane one (f) Plane two

Figure 12: The time staked images are given for the first 5 seconds of each velocity using the mixture of the 100-200 μm, 400-600 μm and 750-1000μm powder (*mix 2*). In these experiments the superficial velocity was reduced for each measurement instead of increasing steps in the superficial velocity. The samples were at (a),(b) 0.29 m/s, (c),(d) 0.31 m/s and (e),(f) 0.35 m/s respectively.

images. In Mammoli, A. A. and Brebbia, C. A., editors, *Computational Methods in Multiphase flow VI*, pages 141–151, Ashurst Lodge, Ashurst, Southampton SO40 7AA, UK. Wessex Institute of Technology, WIT-Press.

Salehi-Nik, N., Sotudeh-Gharebagh, R., Mostoufi, N., Zarghami, R., and Mahjoob, M. (2009). Determination of hydrodynamic behaviour of gas-solid fluidized beds using statistical analysis of acoustic emissions. *International Journal of Multiphase flow*, 35:1011–1016.

Saxena, S., Rao, N., and Tanjore, V. (1993). Diagnostic procedures for establishing the quality of fluidization of gas-solid systems. *Experimental Thermal and Fluid Science*, 6:56–73.

Scheffé, H. (1959). *The analysis of variance*. John Wiley and Sons, Inc., New York.

Sharma, R., Karki, S., and Masoudi, N. (2010). Electrical capacitance tomography for characterising bubbles in fluidized beds. Master's thesis, Telemark University College, Porsgrunn, Norway.

van Biljon, C., du Toit, E., and Nicol, W. (2011). Effect of fines on the bubble properties in a two-dimensional fluidized bed by digital image analysis. In Luckos, A. and den Hoed, P., editors, *Industrial Fluidization South Africa, Supporting sustainable strategies*, pages 267–275, Chamber of Mines Building, 5 Hollard Street, Johannesburg 2017, South Africa. Southern African Institute of Mining and Metallurgy.

Warsito, W. and Fan, L.-S. (2005). Dynamics of spiral bubble plume motion in the entrance region of bubble columns and three-phase fluidized beds using 3d ect. *Chemical Engineering Science*, 60:6073–6084.